JGP Journal of General Physiology

RESEARCH ARTICLE

Rejection of the biophoton hypothesis on the origin of photoreceptor dark noise

Victor I. Govardovskii, Luba A. Astakhova, Alexander Yu. Rotov, and Michael L. Firsov

Rod photoreceptors of the vertebrate retina produce, in darkness, spontaneous discrete current waves virtually identical to responses to single photons. The waves comprise an irreducible source of noise (discrete dark noise) that may limit the threshold sensitivity of vision. The waves obviously originate from acts of random activation of single rhodopsin molecules. Until recently, it was generally accepted that the activation occurs due to the rhodopsin thermal motion. Yet, a few years ago it was proposed that rhodopsin molecules are activated not by heat but rather by real photons generated within the retina by chemiluminescence. Using a high-sensitive photomultiplier, we measured intensities of biophoton emission from isolated retinas and eyecups of frogs (*Rana ridibunda*) and fish (sterlet, *Acipenser ruthenus*). Retinal samples were placed in a perfusion chamber and emitted photons collected by a high-aperture quartz lens. The collected light was sent to the photomultiplier cathode through a rotating chopper so that a long-lasting synchronous accumulation of the light signal was possible. The absolute intensity of bio-emission was estimated by the response of the measuring system to a calibrated light source. The intensity of the source, in turn, was quantified by measuring rhodopsin bleaching with single-rod microspectrophotometry. We also measured the frequency of discrete dark waves in rods of the two species with suction pipette recordings. Expressed as the rate constant of rhodopsin activation, it was 1.2×10^{-11}/s in frogs and 7.6×10^{-11}/s in sterlets. Approximately two thirds of retinal samples of each species produced reliably measurable biophoton emissions. However, its intensity was ≥100 times lower than necessary to produce the discrete dark noise. We argue that this is just a lower estimate of the discrepancy between the hypothesis and experiment. We conclude that the biophoton hypothesis on the origin of discrete dark noise in photoreceptors must be rejected.

Introduction

Rod photoreceptors of the vertebrate retina, in complete darkness, produce random fluctuations of the flowing current. The noise consists of two components. The continuous noise is low-amplitude (few tenths of a pascal) oscillations that are symmetrical with respect to the dark level of the current. It plausibly arises due to spontaneous fluctuations of activity of the phototransduction effector enzyme, cGMP phosphodiesterase (Rieke and Baylor, 1996; Lamb et al., 2018a). The discrete noise consists of randomly occurring high-amplitude (in the range of a few pascals) unipolar current waves. The waves are virtually identical to responses of the rod to single photons (Baylor et al., 1979, 1980). The generation of single photon rods relies on a multistep amplification cascade that, at each step, involves hundreds of molecules; the turnoff of the transduction cascade is also supported by a concerted action of a number of proteins and low-molecular-weight components (Arshavsky and Burns, 2012, 2014; Lamb and Hunt, 2017; Lamb et al., 2018b). It is improbable that such a complex chain of events could be reproduced by random fluctuations in the system unless it is initiated by a single molecule at its very beginning—that is, by activation of rhodopsin.

Until recently, it has been generally accepted that the activation is caused by internal thermal motion of the rhodopsin molecule itself (Baylor et al., 1980; Donner et al., 1990; Barlow et al., 1993; Kefalov et al., 2003; Fu et al., 2008; Luo et al., 2011; Gozem et al., 2012; Guo et al., 2014; Yanagawa et al., 2015; Luk et al., 2016). Therefore, the properties of the discrete dark noise should critically depend on the properties of rhodopsin. Since the discrete waves are identical to responses to real light, they comprise an irreducible source of noise. So, they may limit threshold sensitivity of vision, thus, having a high functional significance. One of the intriguing predictions is that the level of the discrete dark noise should increase when the visual pigment absorbance shifts to a longer wavelength. This is because the energy of long-wavelength photons is lower than the energy of short-wavelength ones, and lower energy for activation is easier

Sechenov Institute of Evolutionary Physiology and Biochemistry Russian Academy of Science, St. Petersburg, Russia.

Correspondence to Victor I. Govardovskii: vgovardovski@yahoo.com.

to obtain from thermal motion. Presumably, a higher rate of thermal activation may explain different sensitivities of rods and cones and preclude the use of red-sensitive visual pigments at low light levels, the proposition known as Barlow's hypothesis (Barlow, 1957). A balance between the sensitivity to ambient light and the noise level might govern the adaptation of visual pigments to specific light environments (Luk et al., 2016). Not surprisingly, a good deal of work has been done to theoretically describe possible underlying intramolecular mechanisms and to predict their impact on visual functions (Luo et al., 2011; Gozem et al., 2012; Yanagawa et al., 2015).

Yet, a few years ago it was proposed that rhodopsin molecules are activated not by heat but rather by real photons generated within the retina by redox reactions—that is, by chemiluminescence (Bókkon and Vimal, 2009; Wang et al., 2011; Li and Dai, 2016; Salari et al., 2016, 2017). The concept of "biophotons" is now widely used to explain a number of other visual phenomena, such as phosphenes and afterimages (Salari et al., 2017) and in more esoteric fields including control of embryonic development, neural transmission, and intelligence (Volodyaev and Beloussov, 2015; Kumar et al., 2016; Wang et al., 2016).

Since the properties of discrete dark noise in rods are well known, a stringent quantitative test of the biophoton hypothesis is possible. Using a wide-spectral-band, high-quantum-yield photomultiplier (PMT; Hamamatsu R9110), we measured intensities of biophoton emission from isolated retinas and eyecups of frogs (*Rana ridibunda*) and fish (sterlet, *Acipenser ruthenus*). Retinal samples were placed in a perfusion chamber, and emitted photons were collected by a high-aperture quartz lens. The absolute intensity of bioemission was estimated by measuring the response of the measuring system to a calibrated light source. The intensity of the source, in turn, was quantified by measuring rhodopsin bleaching with single-rod microspectrophotometry.

Approximately two thirds of samples of each species produced reliably measurable responses. However, the intensity of biophoton emission was ≥100 times lower than necessary to produce the discrete dark waves at the rate determined in independent electrophysiological experiments.

We conclude that the biophoton hypothesis of the origin of discrete dark noise in photoreceptors must be rejected and that the further study of mechanisms of thermal activation of rhodopsin retains its importance.

Materials and methods

Animals and preparations

Adult frogs, *R. ridibunda*, were caught in the wild in southern Russia; juvenile sterlet sturgeons, *A. ruthenus*, were obtained from a local breeder. Frogs were kept for up to 6 mo with free access to water at 10–15°C on a natural day/night cycle and fed mealworms. Fish of 25–30 cm in length were kept in aerated aquaria at 20–22°C on 12/12-h day/night cycle and fed commercial fish food (Tetra Pond Sterlet Sticks). Animals were treated in accordance with the European Communities Council Directive (November 24, 1986; 86/609/EEC), and the protocol was approved by the local Institutional Animal Care and Use Committee. Prior to the experiment, the animals were dark adapted overnight. Animals were decapitated, and their eyes were enucleated under dim red light. All further procedures were conducted at infrared television surveillance. The eyes were hemisected, and, if necessary, the retinas were extracted into Ringer's solution.

Measurements of the biophoton emission

The apparatus was assembled within a light-tight metal box that was placed into an additional black box; the entire setup was situated in a dark room. Light from the sample was collected by a quartz lens of the focal ratio f/d = 0.8. Transmittance of the lens was checked down to 320 nm; an ∼1.25-fold attenuation was seen at the shortest wavelengths compared with the visible part of the spectrum. Combined with the spectral sensitivity of the PMT, it yielded the spectral response shallowly declining from 320 to 825 nm and further sharply dropping in infrared. The typical size of the sample was ∼6 × 8 mm^2, and it was imaged at a magnification of approximately ×1.5 over the 6 × 8–mm^2 photocathode of the PMT. The collected light passed to the PMT through a rotating chopper so that a synchronous accumulation of the light signal was possible. Each chopper turn produced two alternating 0.5-s dark/0.5-s light cycles. Typically, signals from 1,000 chopper turns (2,000 cycles) were averaged. PMT output was low-pass filtered (25-ms simple RC-filter) and sampled at 16-bit resolution at 5-ms intervals. Isolated retinas were attached on the vitreal side to small sheets of white filter paper. Opened eyecups were placed on a wet cotton pad. Then two sorts of samples were used: (1) eyecups or isolated retinas placed on a black background in a wet chamber or (2) isolated retinas placed receptor side up in a perfusion chamber. The chamber was formed by a 0.7-mm-wide gap between two coverslips. Ringer's solution was gravityfed to the inlet of the chamber and sucked out at the outlet. The perfusion rate was ∼0.2 ml/min, which ensured complete solution exchange over the retina in ∼10 s. Measurements were done at room temperature (20–22°C).

Statistical processing of the bioemission recordings

Due to the extremely low intensity of the biophoton emission, the signal cannot always be visually detected in raw unfiltered recordings. Therefore, we primarily selected recordings for further processing by computing the average and SE for dark (0–0.2 s and 0.8–1.0 s, chopper fully closed) and light (0.3–0.7 s, chopper fully open) stretches of the recording. Two transition phases between closed and opened states (0.2–0.3 s and 0.7–0.8 s) were excluded. Recordings were considered to contain a light signal if the average reading during the light phase of the cycle was higher than reading during the dark phase at a 95% confidence level based on Student's t test. Further, the selected recordings were averaged. Low-pass Gaussian filtering can be applied as indicated in figure legends. The zero line in each average was drawn by least-square fit through the dark stretches and subtracted. Reliability and magnitude of the averaged signal were then determined by a t test. In final recordings, t values were >7.2 as indicated in the figures. This corresponds to the probability of a zero hypothesis (no signal) $P < 3.5 \cdot 10^{-11}$.

During averaging multiple recordings, the SEM was computed for each time point; this is represented by the error bars shown in the figures. At the same time, the average of the light phase of each recording was calculated and used for computing the global average and SEM for the biophoton emission (expressed further in figures at the rate of rhodopsin activation).

Location of biophoton production

In principle, any retinal structure could produce ultraweak luminescence that would reach photoreceptor outer segments and activate rhodopsin. However, it is known that the discrete dark waves are registered with equal efficiency from the rods attached to big pieces of the retina and from solitary rods retaining just the ellipsoid and outer segment freely floating in the solution. These observations imply that the source of light emission (if it is responsible for the dark noise) is situated in photoreceptors themselves. Moreover, discrete dark noise could be recorded from isolated truncated rod outer segments (ROSs) provided necessary metabolites are supplied via the opened ROS end (Rieke and Baylor, 1996). This further narrows the location of the biophoton source to the ROS. The conclusion has an important implication for establishing a quantitative relationship between the frequency of discrete dark waves and the extraretinal photon flux available for registration (see Appendix). Alternatively, we also considered the situation when bioemission is produced proximal to the ROS layer, either in photoreceptor bodies or in the inner retina. It did not markedly change our conclusions.

Calibration of the biophoton intensity

Accurate conversion of the signal measured by the PMT into the rate of biophoton production poses a problem. Poorly controllable factors include the efficiency of light collection by the lens, lens transmittance, and most importantly, the quantum gain of the PMT photocathode that is not exactly specified by the maker. To circumvent the problem, we used a calibrating light from a light-emitting diode (LED; emission peak at 505 nm; Marl International Ltd.) that shined on the sample and, after passage through the retina and reflection from the underlying filter paper, reached the PMT via the same optical system as the biophotons did (Fig. 1). Absolute intensity of the calibration light was estimated by measuring rhodopsin bleaching by single-cell microspectrophotometry. Since the LED intensity necessary for producing measurable bleach (bleaching rate of 0.01–0.001/s) is far higher than the rate of dark rhodopsin activation (~10^{-11}/s), the intensity was attenuated by ~$15 \cdot 10^6$–fold with a stack of neutral density filters during the signal calibration. This way of calibration yielded exactly the value of a physiological interest, namely the rate of rhodopsin activation that corresponds to a given PMT output (of course, assuming that the activation is caused by biophotons). Further in the paper, the intensity of luminescence will be expressed in arbitrary units that refer to the bins of the analog-to-digital card that captured the PMT output. Conversion of the unit values to the rate constants of rhodopsin activation that they would produce is considered in detail in the Appendix. Necessary computations were done with Mathcad 13 (PTC).

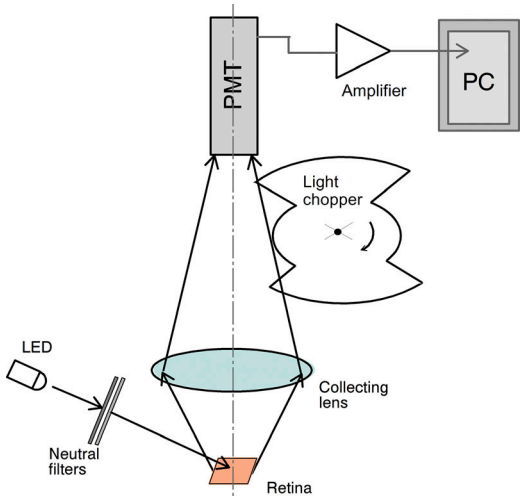

Figure 1. **Schematics of design of the appartus for measuring biophoton emission from the retina.** Light from the retina is collected by a high-aperture lens and sent to the PMT through a rotating chopper so that a synchromous accumulation of the light signal is possible. After amplification, the PMT output is led to a personal computer (PC) via an analog-to-digital converter card. A green (505 nm) LED is used for bleaching the retina and calibrating sensitivity of measurements.

Measurements of discrete dark current noise in single rods

The rate of the dark activation of rhodopsin was determined by suction pipette recordings from single rods, as devised by Baylor et al. (1979). Details of the suction recording rig and the procedure of measurements were described by Astakhova et al. (2008, 2015, 2017). Data acquisition was under the control of LabVIEW (National Instruments) software and hardware. Responses were low-pass filtered at 30 Hz (8-pole analog Bessel filter) and recorded at 2-ms digitization intervals. If necessary, further digital filtering was applied to the recordings.

In most cases, the ratio of the amplitude of discrete dark waves to the continuous noise was high enough to reliably count them by eye. If the signal-to-noise ratio was not good enough, the average discrete dark waves rate was obtained by analysis of the histogram of dark current values (Baylor et al., 1980; Donner et al., 1990; Astakhova et al., 2017).

Solutions

The Ringer's solution for the frogs contained (in mM) 90 NaCl, 2.5 KCl, 1.4 $MgCl_2$, 1.05 $CaCl_2$, 5 $NaHCO_3$, 5 HEPES, 10 glucose, and 0.05 EDTA, pH adjusted to 7.6. For fish, we used 90 NaCl, 2.5 KCl, 1.0 $MgCl_2$, 1.0 $CaCl_2$, 5 $NaHCO_3$, 5 HEPES, and 10 glucose. $MgCl_2$ and $CaCl_2$ as 1 M standard solutions were from Honeywell Fluka. All other chemicals were from Sigma-Aldrich. The temperature was held at 17–19°C.

Recordings were performed from rods attached to small pieces of the retina in the configuration of outer segment in.

Microspectrophotometry

To characterize spectral properties of visual pigments in the frogs and sterlets and to test the functional state of the samples used for bioemission measurements, we performed

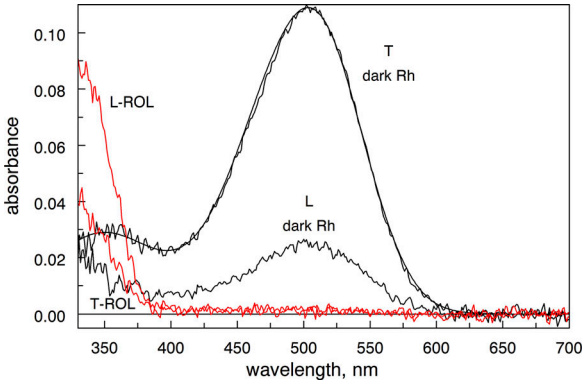

Figure 2. **Testing viability of preparations by rhodopsin photolysis. *R. ridibunda* red rods.** Curves peaking near 500 nm and labeled "dark" show the average of recordings from 15 ROSs from a piece of dark-adapted retina used for bioemission measurements. T and L refer to the polarization of the measuring beam (T, transversal with respect to the ROS axis; L, longitudinal, i.e., parallel to the ROS axis). Curves peaking at <350 nm were recorded from the piece of the same retina that was used for bioemission measurements, bleached in the rig, and left for 30 min in place before preparing the MSP sample. The sharp L-ROL peak at ∼325 nm and the lack of absorbance beyond 400 nm show complete conversion of bleaching products to trans-retinol, thus evidencing a good metabolic state of the sample. Rh, rhodopsin; ROL, all-trans retinol.

microspectrophotometric recordings from solitary ROSs. The design of the instrument, procedures of sample preparation, and measurements were extensively described earlier (Govardovskii et al., 2000; Kolesnikov et al., 2003). Microspectrophotometry was also used to estimate the extent of rhodopsin bleaching by the calibrating LED (Fig. 1) that allowed further converting the PMT output into the equivalent rhodopsin activation rate.

Results

Testing the metabolic state of retinal samples

The supposed biophoton emission should obviously depend on the retinal metabolism. Conditions of our experiments (isolated retina or eyecup in a wet chamber, a perfused retina) are routinely used for recording electroretinogram and other electrical responses of retinal cells; the samples function normally for many hours. Nevertheless, we additionally checked the viability of our samples by measuring the ability of rods to convert all-trans retinal to all-trans retinol after massive rhodopsin bleaching, which critically depends on the metabolic supply of ROSs (Tsina et al., 2004; Chen et al., 2005; Kolesnikov et al., 2007). In the course of the study, the test was done five times on different experimental days. Fig. 2 shows averaged absorbance spectra of ROSs from a dark-adapted retina and from the retina used for the bioemission measurements. The latter was exhaustively bleached in the experimental rig and then left in the rig for an extra 30 min to allow photoproducts to decay. Final products show a pure all-trans retinol peak at 325 nm without any trace of metarhodopsin or all-trans retinal (peak absorbance at 380 nm and shoulder beyond 400 nm), thus evidencing a good functional state of the rods.

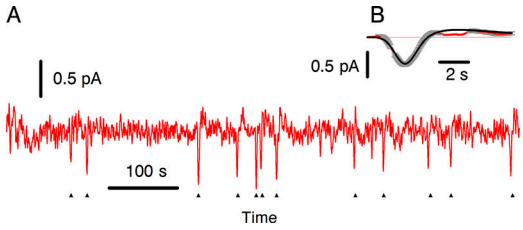

Figure 3. **Dark noise in a *R. ridibunda* rod. (A)** Suction pipette recording from a cell attached to the retinal edge. Putative discrete waves are marked with upward black triangles. Variations of the single-event amplitude are partly caused by the continuous noise and partly by an intrinsic variability of the single-photon responses. **(B)** The red line with gray error bars shows the average of 12 discrete dark waves cut off from the record in A (mean ± SEM). The superimposed black line is the averaged single-photon flash response.

Registration of retinal luminescence

Frog

Frequency of discrete dark waves. A sample of the dark current noise in a frog red rod is shown in Fig. 3. The cell was perfused with the solution containing 2 µM adenylyl cyclase activator forskolin that significantly improved the detectability of discrete waves without affecting their frequency (Astakhova et al., 2017). The results from a few test rods agreed with data we reported earlier. Therefore, we did not conduct extensive measurements in the present study, and further used the average rate of the discrete dark waves from Astakhova et al. (2017). Expressed per unit OS volume, it was (22 ± 2.5) · 10^{-6} µm^{-3}/s, which corresponded to the rate constant of dark activation of 1.2 · 10^{-11} Rh^{-1}/s.

Biophoton emission. Recordings from the frog eyecups and isolated retinas in a wet chamber gave similar results and were pooled. 17 of a total of 25 recordings from 16 samples produced a reliable biophoton signal. Fig. 4 A shows a typical "good" single recording, which was obtained by averaging 2,000 1-s chopper dark-light cycles. Here, the signal is expressed in arbitrary units that correspond to output bins of the analog-to-digital converter card. 10 frog retinas studied in the perfusion chamber produced a weaker signal of approximately one fourth or less of that shown in Fig. 4 A and were not included in the average. Excluding "too weak" signals created a bias in favor of the biophoton hypothesis. This actually strengthens our final conclusion. Presenting average results in arbitrary units is not useful, however. Amplitude of the signal may vary among samples not only due to intrinsic variability of the biophoton emission but also due to a possible difference in the sample area. Therefore, the raw recordings must be converted before averaging into the physiologically relevant and area-independent variable of the rate constant of rhodopsin activation. This was done as follows: (1) On each sample, recording of biophoton emission (I_e) was preceded by recording the intensity of the calibration light reflected from the sample (I_c). Since both I_e and I_c are proportional to the sample area, further normalization to I_c eliminated area dependence. (2) The rate constant of rhodopsin activation by measured biophotons was calculated as

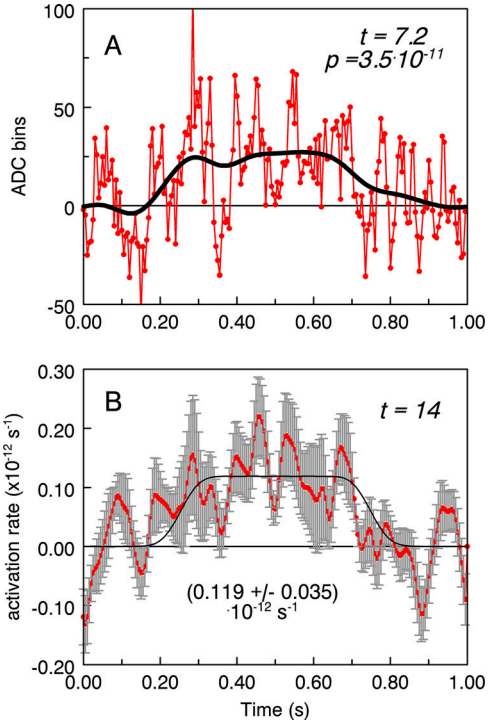

Figure 4. **Intensity of biophoton emission from isolated *R. ridibunda* retinas and eyecups. (A)** The red line with markers shows the raw (digitally unfiltered) experimental recording that represents an average of 2,000 1-s dark-light chopper cycles. Signal values are expressed as analog-to-digital converter (ADC) bins. The thick black line represents the same data Gauss-filtered with a 150-ms window. Results of Student's *t* test for the difference between unfiltered dark (0–0.2 s and 0.8–1.0 s) and light (0.3–0.7 s) periods are shown in the upper right. **(B)** The average of 14 recordings from the five best retinas, each recording including 1,000 or 2,000 cycles. Raw ADC readings are converted to the rates of rhodopsin activation as described in the text (Eq. 1; G = 11.4 for the frog; Fig. 11). Circles and error bars are mean ± SEM. The black line is the response to a higher-intensity calibrating light from the LED that was scaled to show the expected waveform of a noise-free signal. Recordings are smoothed before averaging by a Gaussian filter (25-ms window, *ksmooth* function in Mathcad).

$$r_c = 1 \Big/ Gain \cdot \frac{I_e}{I_c \cdot Att \cdot \tau_{bleach}}. \quad (1)$$

Here, τ_{bleach} is the time constant of rhodopsin bleaching by unattenuated bleaching light, and $Att = 1.47 \cdot 10^7$ is the attenuation of the calibrating light with respect to the bleaching light. The factor *Gain*, ∼5–12, takes into account more favorable conditions of registration of intrinsic bioemission compared with external (bleaching or calibrating) light (see the explanation in the Appendix). Fig. 4 B shows the average rate of dark noise that corresponds to the bioemission detected in our experiments. Its plateau is at $(1.19 \pm 0.35) \cdot 10^{-13}$/s (average ± SEM of 14 best recordings) that is 102 times lower than the rate constant of discrete dark waves in *R. ridibunda* rods ($1.2 \cdot 10^{-11}$/s; Astakhova et al., 2017).

Sterlet

Rod visual pigment. We have chosen *A. ruthenus* to further test the biophoton hypothesis because the level of the rod

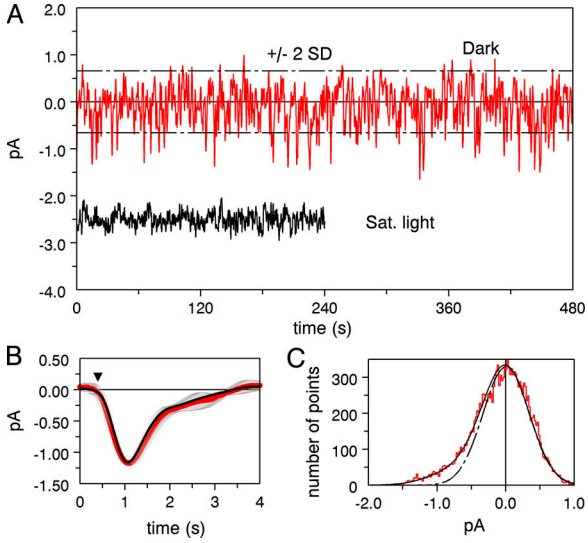

Figure 5. **Suction pipette recordings of continuous and discrete dark noise in an *A. ruthenus* rod. (A)** The red line shows the continuous dark recording low-pass filtered at 3 Hz. The dot-dashed lines show ±2 SDs of the continuous noise; negative peaks crossing the −2-SD level are considered putative discrete waves. The black line shows the instrumental noise isolated by illuminating the cell with saturating light. **(B)** The red line with gray error bars shows the average of 15 discrete waves cut from the dark record in A (mean ± SEM). The superimposed thick black line is the average single-photon flash response of the same rod. **(C)** The red staircase line shows the histogram of dark current values from A. The theoretical fit (continuous black line) is calculated as a convolution of a Gaussian continuous noise (SD = 0.336 pA^2, dot-dashed line) and single-photon responses from B occurring on average once in 9.5 s.

discrete dark noise in sturgeons was found to be almost an order of magnitude higher than in the frog, and it was attributed to their use of far-longer wavelength-sensitive visual pigments (Firsov and Govardovskii, 1990). Indeed, sterlet rods contained porphyropsin (A_2-based pigment) with a maximum absorbance at 545 nm (microspectrophotometry data not shown), close to what has been reported in other sturgeons (Govardovskii et al., 2000; Sillman et al., 2005).

Frequency of discrete dark waves. A sample suction recording from a sterlet rod is shown in Fig. 5, A and B. The continuous 8-min trace in Fig. 5 A clearly demonstrates that the frequency of the discrete dark waves in sterlet is far higher than that in the frog (compare with Fig. 3). If discrete waves are counted as peaks crossing 2-SD level of the continuous noise (marked with dot-dashed lines in Fig. 5 A), it yields one event per 10 s compared with one per 1 min in the frog. The signal-to-noise ratio in the sterlet was a bit lower than in the frog, though, so we applied the histogram analysis to more reliably estimate the rate of the waves production (Fig. 5 C; Baylor et al., 1980; Donner et al., 1990; Astakhova et al., 2017). The average rate of discrete dark waves in the sterlet was derived from recordings on 11 cells. Totally, 757 waves were detected during 9,552 s of recordings, which yielded the rate of dark activation of $7.6 \cdot 10^{-11}$/s, ∼6 times higher than in the frog.

Biophoton emission. 20 isolated retinas and eyecups from 11 fish were studied. 14 of them produced a reliable biophoton

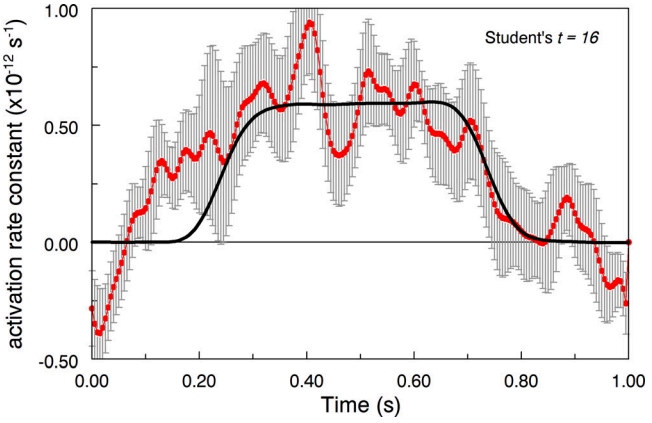

Figure 6. **Biophoton emission from sterlet retina.** The red dots and error bars show average ± SEM of 16 recordings from 12 samples. Raw analog-to-digital readings are converted to the rates of rhodopsin activation as described in the text (Eq. 1; G = 7.1 for sterlet; Fig. 11). The thick black line is the response to a higher-intensity calibrating light from the LED scaled to show the expected waveform of a noise-free signal.

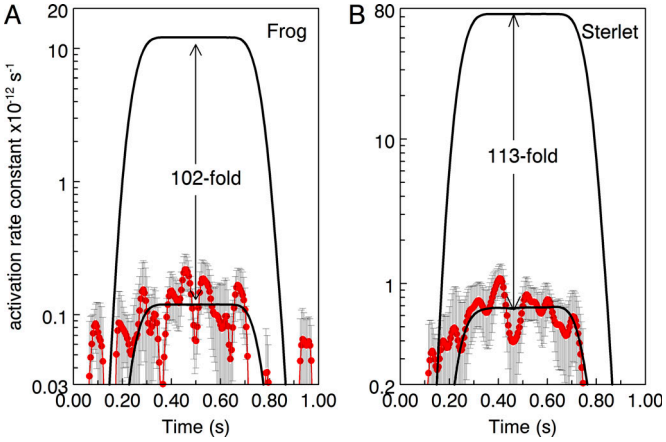

Figure 7. **Comparing biophoton emission with the rate of dark rhodopsin activation derived from electrophysiological recordings. (A)** Frog. **(B)** Sterlet. The red dots with error bars are the average bioemission curves taken from Fig. 4 B and Fig. 6. The high-amplitude black traces show the bioemission signal that would correspond to the actual frequency of discrete dark waves.

signal. The 12 best responses were included in the average. The intensity of biophoton emission expressed as an equivalent dark waves rate was $(0.67 \pm 0.11) \cdot 10^{-12}$/s (Fig. 6). This is approximately sixfold higher than in frog and 113 times lower than the experimentally measured rate of $7.6 \cdot 10^{-11}$/s.

Discussion

We have detected a weak light emission from isolated retinas and eyecups of frogs and fish in general agreement with results reported earlier (Li and Dai, 2016). To determine whether the measured intensity is sufficient to produce discrete dark noise in rods of these species, we calibrated the sensitivity of the measuring system in terms of the rate of rhodopsin bleaching. For this, we partially bleached retinas in the experimental chamber by a separate light source for a fixed period of time and then quantified rhodopsin bleaching by microspectrophotometry on solitary ROSs. Thus, the intensity of an unattenuated bleaching LED can be expressed as the rate constant of rhodopsin bleaching (per second). Further, the light from the LED was attenuated by $1.47 \cdot 10^7$-fold with a stack of neutral density filters, which finally resulted in an $\sim 10^{-9}$/s bleaching rate constant that could vary among experiments. The calibrating light, after reflection from the retina, reached the PMT. Thus, the PMT output can serve as a crude estimate of the rate of rhodopsin activation that would be produced by measured bioemission.

However, conditions of measurements of bleaching and emitted light are different for the external calibrating source and for photons created within the ROS layer or the retina. The optics of the system favors the registration of the bioemission versus calibration lights that would provide the same level of rhodopsin activation in both cases. The situation is described in detail in the Appendix. Computations show that at the same level of rhodopsin activation a 5–12-times stronger signal is expected at the PMT when the bioemission is measured compared with measuring bleaching-equivalent calibration light. The correction made with Eq. 1 allows converting the obtained biophoton signal into the rate of rhodopsin activation (of course, assuming that the calibration light and bioemission peak at the same wavelength close to the rhodopsin absorbance maximum).

Fig. 7 compares the level of the discrete dark noise caused by available biophotons with the level of the noise measured by recordings of the rods' dark current. Bioemission appears >100 times weaker than necessary to account for the physiological discrete dark noise.

Actually, the discrepancy between the assumptions of the biophoton hypothesis and the experimentally measured intensity of bioemission may be far bigger. The above consideration assumed that the bioemission spectrum is similar to the spectrum of our calibration LED (505 nm), that is, peaks at or near the absorbance maximum of the visual pigment. As far as we are aware, there are only vague mentions on the real spectral range of biophotons. Routinely, it is stated that the bioemission lies in the UV portion of the spectrum (Volodyaev and Beloussov, 2015; Salari et al., 2017). If that were the case in rods, it would further increase the discrepancy to 250–400 times because the rhodopsin absorbance between 300 and 400 nm is 2.5–4 times lower than at its maximum (Govardovskii et al., 2000). However, there is an apparently sole report on real measurements of spectral composition of bioemission from brain slices in a few species (frog, chicken, mouse, pig, monkey, and human; Wang et al., 2016). The spectral distribution was not characterized in detail, but it was stated that the average wavelength of emission in frogs lies at ~600 nm and at longer wavelengths in higher vertebrates. Since the absorbance of the frog rhodopsin at 600 nm is ~30 times lower than at its maximum, correspondingly a 30-times brighter 600-nm emission is necessary to produce the bleaching equivalent that is measured at 505 nm. This would increase the discrepancy between the available and necessary light to a few thousand times.

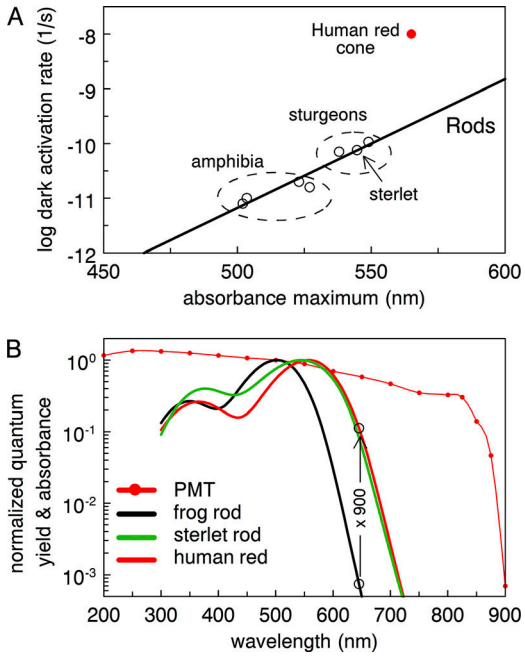

Figure 8. **Relation between spectral sensitivities of visual pigments, their dark noise, and the putative interaction with biophotons. (A)** Dark activation rate as a function of absorbance maximum of rhodopsins. Data for the amphibians are from Baylor et al. (1980), Donner et al. (1990), Fyhrquist et al. (1998), and Astakhova et al. (2017). Data for the sturgeons are from Firsov and Govardovskii (1990) and present paper. The red circle marks the only available experimental point for human red-sensitive cone visual pigment expressed in mouse rods (Fu et al., 2008). **(B)** Comparison of absorbance spectra of some visual pigments and the spectral sensitivity of the R9110 Hamamatsu PMT. Open circles at 645 nm mark the spectral position of bioemission that would ensure the right ratio of cone/rod discrete dark noise (approximately ×1,000).

In apparent favor of the biophoton hypothesis is its potential ability to explain the known general increase of the dark noise with the red shift of the visual pigment absorbance (Firsov and Govardovskii, 1990; Luo et al., 2011; Fig. 8 A). It was routinely attributed to the lower thermal energy necessary to activate more red-sensitive pigments. According to an alternative proposal (Salari et al., 2016, 2017), cones are "noisier" than rods due to their bulky ellipsoids supporting brighter bioemission. The reasoning is flawed. Individual photoreceptors absorb just a small fraction of light emitted by themselves. The rest is spread within the retina and illuminates neighbor receptors of all types. Reciprocally, neighbors illuminate the photoreceptor in question. Therefore, there is a common light field within the retina that equally affects all rods and cones (save a possible difference in spectral sensitivity). The argument is undeniable since human red cone visual pigment produces high discrete dark noise when expressed in a rod along with its native rhodopsin (Fu et al., 2008).

As rods and cones share the same biophoton pool, the difference in their noise levels can be explained by different spectral sensitivities of their visual pigments combined with the biophoton spectrum peaking in red at 640–650 nm (Fig. 8 B). In this case, the same high-intensity red emission would excite red cones ∼1,000 times more efficiently than rods. Yet, to produce proper noise in cones, biophoton emission should then be ∼1,000 times greater than the equivalent rod-activating calibration light at 505 nm. The spectral sensitivity of our measuring system is pretty flat between 500 and 700 nm (Fig. 8 B). Therefore, the corresponding PMT response to rod- and cone-activating light should be 1,000 times stronger than shown in Fig. 7 and nearly five orders of magnitude higher than the signal measured experimentally.

Predictions of the biophoton hypothesis are also inconsistent with the experimental data already published by its proponents. Li and Dai (2016) studied biophoton emission from rat and frog isolated retinas. After estimating the efficiency of light collection by their measuring system, the authors were able to express the data as total emission over a 4π solid angle. Our analysis shows that under optical conditions of measurements made by Li and Dai (2016), the ratio of internally absorbed to externally emitted light is underestimated because the authors did not take into account the complex layered retinal structure and total reflections at interfaces (Appendix and Fig. 9). The correction is in favor of the biophoton hypothesis; the measured values must be multiplied by 2.5 in the frog and by 1.8 in the rat to convert them into equivalent dark activation rates (see Appendix). This translates the value from Li and Dai (2016) for the frog (0.018 photons per rod per minute) into 0.045 dark activations per rod per minute. Since the rate of discrete dark waves is ∼1 per minute per rod (Fig. 3), the measured intensity of bioemission is ≥22 times lower than necessary to produce discrete noise. Besides, Li and Dai (2016) made measurements at 34°C, which would significantly increase the dark noise compared with routine measurements at room temperature. Based on known temperature dependence in toads (Q_{10} = 3.46; Baylor et al., 1980), the expected dark event frequency at 34°C would be ∼5 per minute, that is, 110 times higher than the detected biophoton emission, in surprising agreement with our present result (Fig. 7 A). The biophoton emission measured by Li and Dai (2016) in rats has to be multiplied by 1.8, which yields 0.0027 biophotons absorbed per rod per minute at 36°C. This is 270 times lower than measured discrete dark noise (0.72 per rod per minute, admittedly, obtained in the mouse; Burns et al., 2002; Naarendorp et al., 2010).

Strictly speaking, the title of the article by Li and Dai (2016), "Biophotons Contribute to Retinal Dark Noise," is correct. We confirm that there is a low-level emission of biophotons in the retina, but its contribution to discrete dark noise is not higher than ∼1% and is probably much smaller. We conclude that the biophoton hypothesis on the origin of the photoreceptor dark noise must be rejected.

Appendix

Relation between the rhodopsin activation and registered bioemission or calibration signal

Within the framework of the biophoton hypothesis, redox reactions in the retina produce photons that partly leave the retina, are registered by a measuring system, and are partly absorbed by rhodopsin in ROSs, thus causing discrete dark noise.

The optics of light collection deserves special attention. It is problematic to reliably estimate the sensitivity of the rig

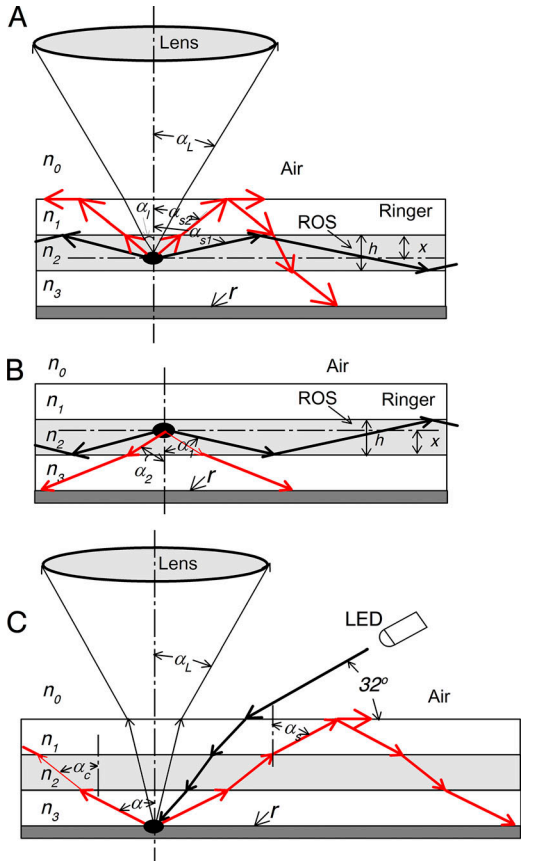

Figure 9. **Propagation of emitted and calibrating light in the retina.** The sample is treated as a three-layered structure: the perfusing Ringer's solution, a layer of ROSs, and an inner retina with vitreous. The corresponding refraction indices are $n_1 = n_3 = 1.34$ and $n_2 = 1.39$. The dark bottom layer shows the filter paper under the sample. **(A)** Biophotons emitted within the upper hemisphere from various depth x in the ROS layer. **(B)** Biophotons emitted within the lower hemisphere. **(C)** Calibrating or bleaching light comes from the LED, crosses the retina, is diffusely reflected from the bottom, crosses the retina again, and is partly transmitted to the measuring system. A detailed explanation is in the Appendix.

based on the efficiency of light collection by the optical system, absolute PMT sensitivity, and other poorly assessed experimental parameters. To circumvent the problem, we included in the apparatus a calibrating light source. A bright LED (505 nm) was used to bleach rhodopsin in situ, and the level of bleaching was quantified by single-rod microspectrophotometry. This way, we calibrated the intensity of the LED in physiologically relevant units, that is, as the rate of rhodopsin bleaching (activation) it produces. Then the properly attenuated LED light was used to calibrate the sensitivity of the measuring system.

Still, the situation is not that simple. Paths of bleaching and escaping lights are different for the external calibrating source and for presumed photons created within the ROS layer. Bleaching (calibrating) light passes through the retina with absorption, diffusely reflects from rather poorly reflecting background, and passes the retina again on the way to the measuring system (Fig. 9 C). On the other hand, the bioemission occurs within the ROS layer, supposedly uniformly along the ROS

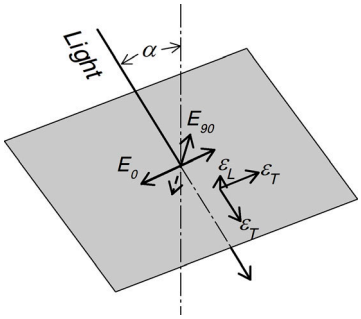

Figure 10. **Interaction of nonpolarized light falling obliquely (at angle α) on photoreceptor membrane with rhodopsin.** The light is considered consisting of two equal-magnitude components, E_0 and E_{90}. E_0 is parallel to the membrane plane; E_{90} is perpendicular to E_0 and to the direction of light propagation. Randomly orientated absorbing dipoles of rhodopsin are represented by two mutually perpendicular components ε_T laying in the membrane plane and a smaller component ε_L perpendicular to it.

(Fig. 9 A). Half of the light is emitted upward within 2π solid angle and reaches the registration system after partial absorption on the way. The other half is emitted downward, reflects from the background, and reaches the PMT after the second passage through the retina (Fig. 9 B). Thus, the calibrating light is attenuated by two passages through the entire thickness of the ROS layer and by reflection from the background before reaching the PMT. If the background reflectance were zero, ideally no light would be detected. On the other hand, half of the bioluminescent light (save the absorption by rhodopsin) is always registered independently of the reflection from the background. Therefore, the optics of the system favors the registration of the bioemission versus calibration light at the same level of rhodopsin activation in both cases.

Light absorption by rhodopsin in the ROS layer

Specific absorbance for light propagating at various angles α in the ROS layer ($\varepsilon(\alpha)$) is one of the key parameters of the model. (From here and onward, the angle α is measured with respect to the ROS axis, that is, from normal to the retinal surface). Specific absorbance is commonly expressed as the optical density per micron of the light path. Absorption of light by rhodopsin can be characterized by two absorbing dipoles, one lying parallel to the plane of disk membranes (ε_T) and the other perpendicular to the plane (ε_L; Fig. 10). Since rhodopsin rotates within the membrane, ε_T can be considered to consist of two mutually perpendicular components. The same $\varepsilon_T = \varepsilon_0$ is measured side-on (α = 90°) by using linearly polarized light whose electric vector is parallel to the plane of the membrane, that is, transversal to the ROS axis (T-orientation). Side-on measurements with light polarized along the ROS axis (L-orientation) yield $\varepsilon_L < \varepsilon_T$. The dichroic ratio $DR = \varepsilon_T/\varepsilon_L$ is usually 3.5–5. The specific absorbance of nonpolarized light propagating at an arbitrary angle α is given by

$$\varepsilon(\alpha) := \varepsilon 0 \frac{\left(1 + cos(\alpha)^2\right) + \frac{sin(\alpha)^2}{DR}}{2}. \quad (2)$$

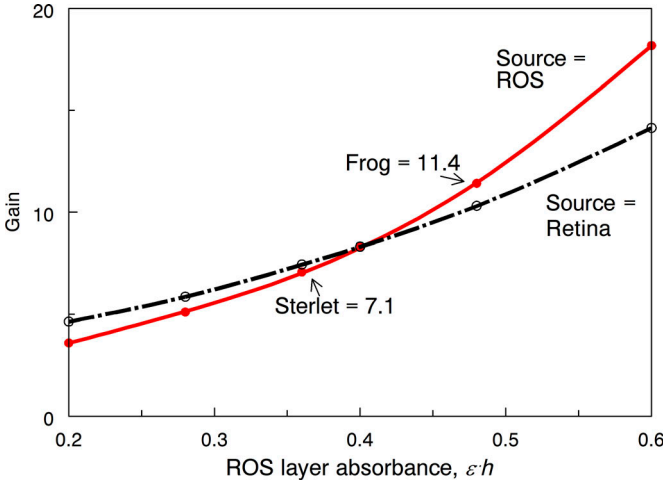

Figure 11. **Advantage of measuring bioemission vs. calibrating light both producing the same level of rhodopsin activation.** The advantage *Gain* is defined in the Appendix, Eq. 12. The red line represents biophotons produced in ROSs. The black line represents the sources of biophotons proximal to ROSs.

ε_0 was estimated in the frog and sterlet by microspectrophotometry. Registered absorbance at 505 nm in each individual rod was divided by the ROS diameter taken from cell images captured with the MSP infrared television system. Averaged data yielded ε_0. It was (0.015 ± 0.0004)/μ in the frog (mean ± SEM of 20 ROSs). Molar extinction of the A_2-based sterlet porphyropsin is ∼25% lower than in the frog A_1-rhodopsin, which accounts for the lower ε_0, (0.0115 ± 0.0003)/μ, in the sterlet. Bulk ε for propagation in the ROS layer is still lower because of the relatively loose packing of ROSs that occupy ∼80% of the volume. Hence, we assume ε_0 = 0.012/μ in the frog and ε_0 = 0.009/μ in the sterlet. Besides, specific absorbance enters further equations as a product $\varepsilon_0 \times h$ where h is the thickness of the ROS layer (in micrometers). On average, ROSs in the sterlet were a bit shorter than in the frog (35 vs. 40 μm). This was taken into account when plotting Fig. 11.

Transmission and absorption of bioemission in retinal layers. Fig. 9, A and B, shows the optics of the collection of the bioemission generated within the ROSs. We treat the sample as a three-layered structure consisting of the ROS layer sandwiched between a film of Ringer's solution on the upper surface and inner retina with Ringer's solution underneath. It is assumed that the biophotons are emitted uniformly in all directions over 4π solid angle at unit intensity per unit retinal thickness and unit area per steradian. The term *amount* will further be used for a measure of light flux that can be expressed as a number of photons, energy, etc. All amounts of transmitted and absorbed light are further normalized to 2π and retinal thickness h, that is, expressed as fractions of the total one-side emission. We also use the terms *transmittance* and *absorptance* that mean *fractions* of the *amount* transmitted through or absorbed in a retinal layer.

The fate of the light emitted in the upper hemisphere toward the registration system is shown in Fig. 9 A. A fraction of light propagates outside the Snell window at the ROS/Ringer's solution interface (angle α_{s1}). It is captured within the ROS layer due to multiple total reflections at its borders and is absorbed completely. The absorbed amount $A_{up1} = sin(arccos(n_1/n_2)) = 0.266$.

Angle $\alpha_{s2} = arcsin(n_0/n2)$ is the angle of total reflection at the Ringer's solution/air interface. The light that propagates between the angles α_{s1} and α_{s2} undergoes total reflection here, crosses the ROS layer again, and reaches the reflecting filter paper at the bottom. Its total amount (absorbed and transmitted) is $\cos(\alpha_{s2}) - \cos(\alpha_{s1}) = 0.429$. The absorbed fraction A_{up2} is calculated as follows.

The absorbed fraction of light that is emitted at a depth x in the ROS layer is:

$$A_1(\alpha,\ x) = 1 - 10^{-\varepsilon(\alpha)\frac{x}{\cos(\alpha)}}. \quad (3)$$

If the light undergoes total reflection and crosses the full-thickness h of the ROS layer again, as in Fig. 9 A, Eq. 3 is substituted by

$$A_2(\alpha,\ x) = 1 - 10^{-\varepsilon(\alpha)\frac{x+h}{\cos(\alpha)}}. \quad (4)$$

The total amount of light absorbed between two Snell windows is obtained by integrating Eq. 4 over $x = 0$ to h and over $\alpha = \alpha_{s1}$ to α_{s2}:

$$A_{up2} = \frac{1}{h}\int_{\alpha_{s2},0}^{\alpha_{s1},h} A_2(\alpha, x) \cdot \sin(\alpha) \cdot d\alpha \cdot dx. \quad (5)$$

The amount transmitted to the bottom is $T_{dwn1} = 0.429 - A_{up2}$.

The rest of the light emitted upward within the Snell window α_{s2} is partly absorbed and partly transmitted toward the measuring system. The absorbed amount is

$$A_{up3} = \frac{1}{h}\int_{\alpha_{0},0}^{\alpha_{s2},h} A_1(\alpha, x) \cdot \sin(\alpha) \cdot d\alpha \cdot dx. \quad (6)$$

The lens collects light from the angle $\alpha_L = arctan(R/L)$. Here R = 20 mm is the radius of the lens, and L = 35 mm is its distance from the retinal sample. Within the ROS layer, the limiting angle $\alpha_l = \arcsin((\sin(a_L) * \frac{n0}{n2})$. The amount of light transmitted to the lens and available for measurement is

$$T_{up1} = \frac{1}{h}\int_{0,0}^{\alpha_l,h} (1 - A_1(\alpha, x)) \cdot \sin(\alpha) \cdot d\alpha \cdot dx. \quad (7)$$

The propagation of light emitted by ROSs in the downward direction is shown in Fig. 9 B. Actually, the ROS layer lies on the multilayered inner retina with changing refraction indices $>n_1$. Yet, there is a thin layer of vitreous body and Ringer's solution below the retina. Its refraction index $n_3 = n_1$. It can be shown that it is n_3 that defines the angle α_{s2} of total reflection at which the light returns back to the ROS layer for absorption. Therefore, similarly to the upward propagation, the amount $A_{dwn1} = A_{up1} = sin(arccos(n_3/n_2)) = 0.266$ is completely absorbed in ROSs. The amount emitted within the Snell window α_{s2} is equal to $1 - A_{dwn1} = 0.734$. A part of it is absorbed:

$$A_{dwn2} = \frac{1}{h}\int_{0,0}^{\alpha_{s2},h} A_1(\alpha, x) \cdot \sin(\alpha) \cdot d\alpha \cdot dx. \quad (8)$$

The rest is transmitted to the reflecting bottom, $T_{dwn2} = 1 - A_{dwn1} - A_{dwn2}$.

Thus, the total amount of light emitted in ROSs and reaching the reflecting bottom is $T_{dwntot} = T_{dwn1} + T_{dwn2}$. After diffuse reflection from the bottom into 2π solid angle, $r \times T_{dwntot}$ reaches the ROS layer. Here $r = 0.3$ is the reflection coefficient of wet filter paper placed under the retina. Reflected light coming at an angle α to the vertical axis crosses the ROS layer at the angle $\alpha_c(\alpha) = asin(sin(\alpha) \cdot n_1/n_2)$ (Fig. 9 C). Notice that the light that leaves the ROS layer outside the Snell window at the Ringer's solution/air interface (red arrows) is reflected back and crosses the ROS layer again. Thus its absorption path is doubled, which causes the second term in Eq. 9. After the two passages, the reflected light comes back to the bottom and is partly reemitted. This fraction comprises <3% of measured light and is neglected.

Correspondingly, the overall absorption coefficient for crossing the ROSs layer is

$$f_{abs} = \int_0^{\alpha_s} \left(1 - 10^{-\varepsilon(\alpha_c(\alpha))\frac{h}{\cos(\alpha)}}\right) \cdot \sin(\alpha) \cdot d\alpha + \int_{\alpha_s}^{\frac{\pi}{2}} \left(1 - 10^{-\varepsilon(\alpha_c(\alpha))\frac{2h}{\cos(\alpha)}}\right) \cdot \sin(\alpha) \cdot d\alpha. \quad (9)$$

The amount of light coming from the bottom and absorbed in ROSs = $r \cdot f_{abs} \cdot T_{dwntot}$.

The transmission coefficient for the reflected light reaching the collecting lens is

$$f_{tr} = \int_0^{\alpha_l} 10^{-\varepsilon(\alpha_c)\frac{h}{\cos(\alpha_c(\alpha))}} \cdot \sin(\alpha) \cdot d\alpha. \quad (10)$$

The amount of reflected light passed to the lens = $f_{tr} \cdot r \cdot T_{dwntot}$.

The sum of all components of the absorbed bioemission light is $\Sigma A_e = A_{up1} + A_{up2} + A_{up3} + A_{dwn1} + A_{dwn2} + r \cdot f_{abs} \cdot T_{dwntot}$. The light available for measurment is $\Sigma M_e = T_{up1} + f_{tr} \cdot r \cdot T_{dwntot}$.

Absorption and collection of the calibrating light

Light paths of the bleaching or calibrating light from the LED is shown in Fig. 9 C. The light falls on the retinal surface at the angle 32° (with respect to the retinal plane) and after refractions at interfaces passes the ROS layer obliquely at the angle $\alpha_t = arcsin((cos(32°)/n_2/n_0)) = 55°$. The absorbed amount is

$$A_{Cal1} = 1 - 10^{-\varepsilon(\alpha_t)\frac{h}{\cos(\alpha_t)}}, \quad (11)$$

and the transmitted amount $T_{Cal1} = 1 - A_{Cal1}$. The fraction $r = 0.3$ of the transmitted light diffusely reflects from the bottom and goes toward the ROS layer and the measuring system. The situation is identical to that with reflected biophotons, so Eqs. 9 and 10 apply to computing its absorbed (A_{Cal2}) and measured (T_{upC}) fractions, respectively.

The sum of all components of the absorbed calibration light is $\Sigma A_{Cal} = A_{Cal1} + A_{Cal2}$. The calibration light available for measurement is $M_{Cal} = T_{upCal}$.

The ratio

$$Gain = \frac{\Sigma Me/\Sigma Ae}{Mcal/\Sigma Acal} \quad (12)$$

shows the advantage of measuring bioemission versus calibrating light provided that in both cases rhodopsin activation is the same. Obviously, *Gain* is a function of the specific density of the visual pigment in the ROS layer (ε) and the thickness of the layer *h*. The corresponding curve is shown in Fig. 11 (solid red line).

Absorption and transmission of biophotons produced proximally to outer segments

Although there is a good experimental reason to place the noise-producing biophoton emission into ROSs (see Materials and methods), we also considered the possibility that the bioemission originates in the retina proximally to the ROS layer. Then the situation is similar to the absorption, transmission, and detection of the light diffusely reflected from the bottom. Correspondingly, Eqs. 9 and 10 apply. The resulting *Gain* versus Absorbance curve is shown in Fig. 11 by the broken black line.

Acknowledgments

Support was provided by the Russian Foundation for Basic Research (17-04-00807 to V. Govardovskii).

The authors declare no competing financial interests.

Author contributions: V.I. Govardovskii: conceptualization, funding acquisition, conducting experiments, data processing, writing the draft manuscript. L.A. Astahova: conducting electrophysiological experiments, data processing and discussion, reviewing and editing of the draft manuscript. A. Yu. Rotov: Conducting microspectrophotometric and morphometric measurements, data processing and discussion, review and editing of the draft manuscript. M.L. Firsov: Designing and conducting electrophysiological experiments, software development, data processing and discussion, review and editing of the draft manuscript.

Edward N. Pugh served as guest editor.

Submitted: 27 December 2018
Accepted: 29 March 2019

References

Arshavsky, V.Y., and M.E. Burns. 2012. Photoreceptor signaling: supporting vision across a wide range of light intensities. *J. Biol. Chem.* 287: 1620–1626. https://doi.org/10.1074/jbc.R111.305243

Arshavsky, V.Y., and M.E. Burns. 2014. Current understanding of signal amplification in phototransduction. *Cell. Logist.* 4:e29390. https://doi.org/10.4161/cl.29390

Astakhova, L.A., M.L. Firsov, and V.I. Govardovskii. 2008. Kinetics of turn-offs of frog rod phototransduction cascade. *J. Gen. Physiol.* 132:587–604. https://doi.org/10.1085/jgp.200810034

Astakhova, L., M. Firsov, and V. Govardovskii. 2015. Activation and quenching of the phototransduction cascade in retinal cones as inferred from electrophysiology and mathematical modeling. *Mol. Vis.* 21: 244–263.

Astakhova, L.A., D.A. Nikolaeva, T.V. Fedotkina, V.I. Govardovskii, and M.L. Firsov. 2017. Elevated cAMP improves signal-to-noise ratio in amphibian rod photoreceptors. *J. Gen. Physiol.* 149:689–701. https://doi.org/10.1085/jgp.201611744

Barlow, H.B. 1957. Purkinje shift and retinal noise. *Nature.* 179:255–256. https://doi.org/10.1038/179255b0

Barlow, R.B., R.R. Birge, E. Kaplan, and J.R. Tallent. 1993. On the molecular origin of photoreceptor noise. *Nature.* 366:64–66. https://doi.org/10.1038/366064a0

Baylor, D.A., T.D. Lamb, and K.-W. Yau. 1979. The membrane current of single rod outer segments. *J. Physiol.* 288:589–611. https://doi.org/10.1113/jphysiol.1979.sp012715

Baylor, D.A., G. Matthews, and K.-W. Yau. 1980. Two components of electrical dark noise in toad retinal rod outer segments. *J. Physiol.* 309:591–621. https://doi.org/10.1113/jphysiol.1980.sp013529

Bókkon, I., and R.L.P. Vimal. 2009. Retinal phosphenes and discrete dark noises in rods: a new biophysical framework. *J. Photochem. Photobiol. B.* 96:255–259. https://doi.org/10.1016/j.jphotobiol.2009.07.002

Burns, M.E., A. Mendez, J. Chen, and D.A. Baylor. 2002. Dynamics of cyclic GMP synthesis in retinal rods. *Neuron.* 36:81–91. https://doi.org/10.1016/S0896-6273(02)00911-X

Chen, C., E. Tsina, M.C. Cornwall, R.K. Crouch, S. Vijayaraghavan, and Y. Koutalos. 2005. Reduction of all-*trans* retinal to all-*trans* retinol in the outer segments of frog and mouse rod photoreceptors. *Biophys. J.* 88: 2278–2287. https://doi.org/10.1529/biophysj.104.054254

Donner, K., M.L. Firsov, and V.I. Govardovskii. 1990. The frequency of isomerization-like 'dark' events in rhodopsin and porphyropsin rods of the bull-frog retina. *J. Physiol.* 428:673–692. https://doi.org/10.1113/jphysiol.1990.sp018234

Firsov, M.L., and V.I. Govardovskii. 1990. Dark noise of visual pigments with different absorbance maxima. Сенсор. системы. 4:25–33 (in Russian).

Fu, Y., V. Kefalov, D.-G. Luo, T. Xue, and K.-W. Yau. 2008. Quantal noise from human red cone pigment. *Nat. Neurosci.* 11:565–571. https://doi.org/10.1038/nn.2110

Fyhrquist, N., V. Govardovskii, C. Leibrock, and T. Reuter. 1998. Rod pigment and rod noise in the European toad *Bufo bufo*. *Vision Res.* 38:483–486. https://doi.org/10.1016/S0042-6989(97)00177-6

Govardovskii, V.I., N. Fyhrquist, T. Reuter, D.G. Kuzmin, and K. Donner. 2000. In search of the visual pigment template. *Vis. Neurosci.* 17:509–528 https://www.ncbi.nlm.nih.gov/pubmed/11016572. https://doi.org/10.1017/S0952523800174036

Gozem, S., I. Schapiro, N. Ferré, and M. Olivucci. 2012. The molecular mechanism of thermal noise in rod photoreceptors. *Science.* 337: 1225–1228. https://doi.org/10.1126/science.1220461

Guo, Y., S. Sekharan, J. Liu, V.S. Batista, J.C. Tully, and E.C.Y. Yan. 2014. Unusual kinetics of thermal decay of dim-light photoreceptors in vertebrate vision. *Proc. Natl. Acad. Sci. USA.* 111:10438–10443. https://doi.org/10.1073/pnas.1410826111

Kefalov, V., Y. Fu, N. Marsh-Armstrong, and K.-W. Yau. 2003. Role of visual pigment properties in rod and cone phototransduction. *Nature.* 425: 526–531. https://doi.org/10.1038/nature01992

Kolesnikov, A.V., E.Yu. Golobokova, and V.I. Govardovskii. 2003. The identity of metarhodopsin III. *Vis. Neurosci.* 20:249–265. https://doi.org/10.1017/S0952523803203047

Kolesnikov, A.V., P. Ala-Laurila, S.A. Shukolyukov, R.K. Crouch, B. Wiggert, M.E. Estevez, V.I. Govardovskii, and M.C. Cornwall. 2007. Visual cycle and its metabolic support in gecko photoreceptors. *Vision Res.* 47: 363–374. https://doi.org/10.1016/j.visres.2006.08.024

Kumar, S., K. Boone, J. Tuszyński, P. Barclay, and C. Simon. 2016. Possible existence of optical communication channels in the brain. *Sci. Rep.* 6: 36508. https://doi.org/10.1038/srep36508

Lamb, T.D., and D.M. Hunt. 2017. Evolution of the vertebrate phototransduction cascade activation steps. *Dev. Biol.* 431:77–92. https://doi.org/10.1016/j.ydbio.2017.03.018

Lamb, T.D., M. Heck, and T.W. Kraft. 2018a. Implications of dimeric activation of PDE6 for rod phototransduction. *Open Biol.* 8:180076. https://doi.org/10.1098/rsob.180076

Lamb, T.D., H.R. Patel, A. Chuah, and D.M. Hunt. 2018b. Evolution of the shut-off steps of vertebrate phototransduction. *Open Biol.* 8:170232. https://doi.org/10.1098/rsob.170232

Li, Z., and J. Dai. 2016. Biophotons Contribute to Retinal Dark Noise. *Neurosci. Bull.* 32:246–252. https://doi.org/10.1007/s12264-016-0029-6

Luk, H.L., N. Bhattacharyya, F. Montisci, J.M. Morrow, F. Melaccio, A. Wada, M. Sheves, F. Fanelli, B.S.W. Chang, and M. Olivucci. 2016. Modulation of thermal noise and spectral sensitivity in Lake Baikal cottoid fish rhodopsins. *Sci. Rep.* 6:38425. https://doi.org/10.1038/srep38425

Luo, D.-G., W.W.S. Yue, P. Ala-Laurila, and K.-W. Yau. 2011. Activation of visual pigments by light and heat. *Science.* 332:1307–1312. https://doi.org/10.1126/science.1200172

Naarendorp, F., T.M. Esdaille, S.M. Banden, J. Andrews-Labenski, O.P. Gross, and E.N. Pugh Jr. 2010. Dark light, rod saturation, and the absolute and incremental sensitivity of mouse cone vision. *J. Neurosci.* 30: 12495–12507. https://doi.org/10.1523/JNEUROSCI.2186-10.2010

Rieke, F., and D.A. Baylor. 1996. Molecular origin of continuous dark noise in rod photoreceptors. *Biophys. J.* 71:2553–2572. https://doi.org/10.1016/S0006-3495(96)79448-1

Salari, V., F. Scholkmann, I. Bokkon, F. Shahbazi, and J. Tuszynski. 2016. The physical mechanism for retinal discrete dark noise: Thermal activation or cellular ultraweak photon emission? *PLoS One.* 11:e0148336. https://doi.org/10.1371/journal.pone.0148336

Salari, V., F. Scholkmann, R.L.P. Vimal, N. Császár, M. Aslani, and I. Bókkon. 2017. Phosphenes, retinal discrete dark noise, negative afterimages and retinogeniculate projections: A new explanatory framework based on endogenous ocular luminescence. *Prog. Retin. Eye Res.* 60:101–119. https://doi.org/10.1016/j.preteyeres.2017.07.001

Sillman, A.J., A.K. Beach, D.A. Dahlin, and E.R. Loew. 2005. Photoreceptors and visual pigments in the retina of the fully anadromous green sturgeon (Acipenser medirostrus) and the potamodromous pallid sturgeon (Scaphirhynchus albus). *J. Comp. Physiol. A Neuroethol. Sens. Neural Behav. Physiol.* 191:799–811. https://doi.org/10.1007/s00359-005-0004-6

Tsina, E., C. Chen, Y. Koutalos, P. Ala-Laurila, M. Tsacopoulos, B. Wiggert, R.K. Crouch, and M.C. Cornwall. 2004. Physiological and microfluorometric studies of reduction and clearance of retinal in bleached rod photoreceptors. *J. Gen. Physiol.* 124:429–443. https://doi.org/10.1085/jgp.200409078

Volodyaev, I., and L.V. Beloussov. 2015. Revisiting the mitogenetic effect of ultra-weak photon emission. *Front. Physiol.* 6:241. https://doi.org/10.3389/fphys.2015.00241

Wang, C., I. Bókkon, J. Dai, and I. Antal. 2011. Spontaneous and visible light-induced ultraweak photon emission from rat eyes. *Brain Res.* 1369:1–9. https://doi.org/10.1016/j.brainres.2010.10.077

Wang, Z., N. Wang, Z. Li, F. Xiao, and J. Dai. 2016. Human high intelligence is involved in spectral redshift of biophotonic activities in the brain. *Proc. Natl. Acad. Sci. USA.* 113:8753–8758. https://doi.org/10.1073/pnas.1604855113

Yanagawa, M., K. Kojima, T. Yamashita, Y. Imamoto, T. Matsuyama, K. Nakanishi, Y. Yamano, A. Wada, Y. Sako, and Y. Shichida. 2015. Origin of the low thermal isomerization rate of rhodopsin chromophore. *Sci. Rep.* 5:11081. https://doi.org/10.1038/srep11081